*Graphical Abstract

Flood classification

Pluvial floods

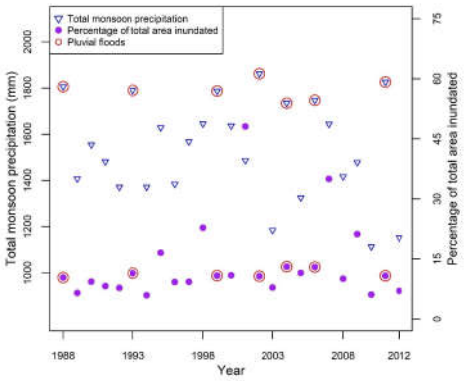

Fluvio-tidal floods

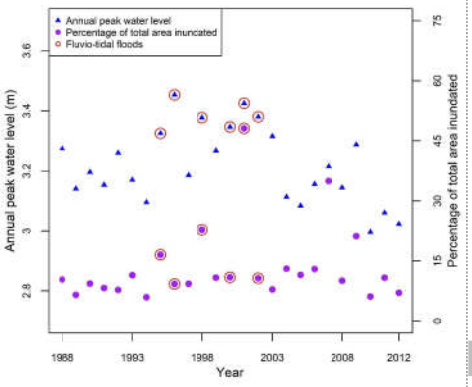

Surge floods

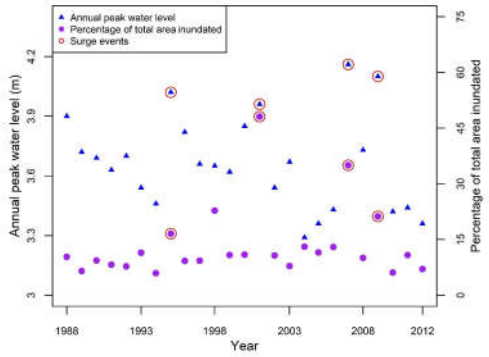

Polders' effectiveness

Pluvial floods

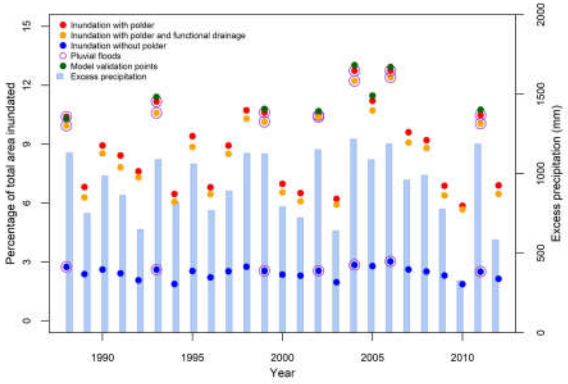

Fluvio-tidal flood (1998)

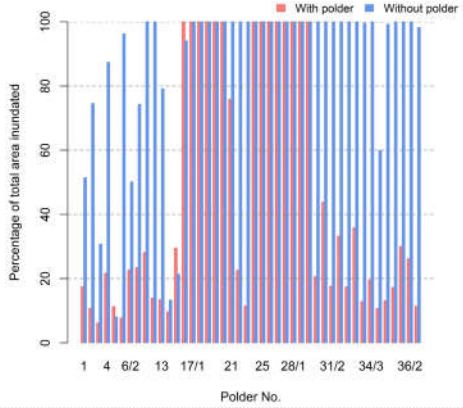

Surge flood (2007)

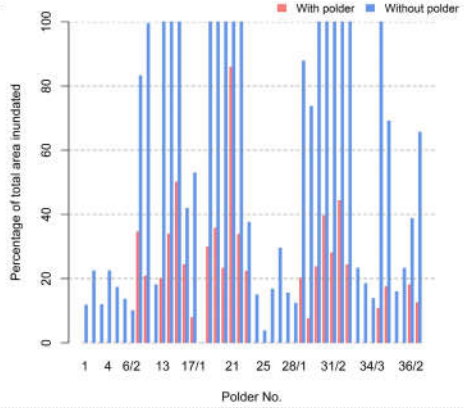

***Highlights (for review : 3 to 5 bullet points (maximum 85 characters including spaces per bullet point)**

- We analysed floods in the coastal zone in Bangladesh in every year within 1988-2012
- Pluvial flooding resulted in 11.4% of the domain being flooded, on average
- Fluvio-tidal and surge floods were less frequent but caused more inundation
- Construction of the polders has increased the extent of pluvial flooded area
- Polders have provided some protection against storm surges and fluvio-tidal events

Have coastal embankments reduced flooding in Bangladesh?

Abstract

From the 1960s, embankments have been constructed in south western coastal region of Bangladesh to provide protection against flooding, but the success of the polder programme is disputed. We present analysis of floods during the years 1988-2012, diagnosing whether the floods were attributable to monsoonal precipitation (pluvial flooding), high upstream river discharge into the tidal delta (fluvio-tidal flooding), or cyclone-induced storm surges. We find that pluvial flooding was the most frequent, but typically resulted in less flooded area (11.44% of the region on average) compared with the other forms of flooding. The greatest area of inundation (48% of total area) occurring in 2001 as a consequence of fluvio-tidal and surge flooding, whilst cyclone Sidr in 2007 flooded 35% of the area. We modelled these different forms of inundation to estimate what flooding might have been had the polders not been constructed. For the 'no embankment' counter-factual scenario, our model demonstrated that because of a combination of subsidence and inadequate drainage, construction of the polders has increased the pluvial flooded area by 6.5% on average (334 km^2). However, during the 1998 fluvio-tidal flood, the embankments protected an estimated 54% of the area from flooding. During the cyclone Sidr storm surge event, embankment failure in several polders and pluvial inundation resulted in 35% area inundation, otherwise, the total inundation would have been 18% area. We conclude that whilst polders have provided protection against storm surges and fluvio-tidal events of moderate severity, they have exacerbated more frequent pluvial flooding and promoted potential flooding impacts during the most extreme storm surges.

Key words: Bangladesh coastal embankment; extreme events; flood classification; pluvial flood; fluvio-tidal flood; storm surge flood

1. Introduction

Structural flood defence systems are one response to flood hazards (Bamberg et al., 2017). While embankments, levees and dikes usually provide flood protection up to a given severity of flooding, these structures are costly and may exacerbate flooding under some circumstances, as well as potentially encouraging the build-up of exposed people and assets (Hui et al., 2016).

Due to the deltaic geographical setting and high population density, Bangladesh is well-known as being vulnerable to flooding (Islam et al., 2016b; Moniruzzaman, 2012). The coastal region is subject to multiple flood hazards, including pluvial floods, which are inundations induced by monsoon precipitation, fluvio-tidal floods and storm surge-induced floods (Abedin and Shaw, 2015; Alam et al., 2017; Brouwer et al., 2007; Haque et al., 2018; Islam et al., 2016a). The impact of several catastrophic floods impelled the Bangladesh government to construct coastal embankments in the 1960s to protect agricultural land and communities (Nishat et al., 2010; Paul and Rashid, 2017; Rahman and Salehin, 2013). Coastal embankments have compartmentalized a portion of coastal region into polders. Their construction was accompanied by the excavation of drainage channels and sluice gates to impede salt water intrusion in the dry season, drain excessive rain water, and allow fresh river water flow to polders in the wet season for irrigation purposes (Masud et al., 2018).

The coastal embankment programme had a profound influence on the geomorphology of the coastal zone, as well as contributing to a transformation in human settlement patterns. The embanked region experienced rapid land use change (Abdullah et al., 2019; Akber et al., 2018). In the last couple of decades, a substantial growth in shrimp farming, replacing agricultural lands, is reportedly associated with soil salinity promoted by the intrusion of saline water in polders (Mukhopadhyay et al., 2018). Moreover, storm surges and pluvial flooding inundated agricultural lands, which has been reflected in a net reduction in land use

for agriculture (Khan et al., 2015). In this naturally dynamic sediment system, reducing flow in the channels of the delta, due to the separation of upstream river 'Mathabhanga' from the river Ganges, caused siltation in the riverbed (Alam et al., 2017). Polders simultaneously also impeded sedimentation within embanked region and resulted in land subsidence inside the polders (Auerbach et al., 2015). As a result of reduced sediment supply or irregular sedimentation, compaction of sediment, and anthropogenic activities (e.g. shrimp farming) (Brammer, 2014; Brown and Nicholls, 2015), the coastal region on average experienced about 2-3 mm/year of land subsidence (Brown and Nicholls, 2015). In addition, physical deterioration and unreliable operation of the sluice gates caused prolonged inundation during the monsoon period (Auerbach et al., 2015; Choudhury et al., 2004; Van Staveren et al., 2017). The earthen embankments are subject to riverbank erosion which can breach the polders, a process that can be exacerbated by tropical cyclones and lead to extensive flood damage (Bhuiyan and Dutta, 2012; Haque and Nicholls, 2018). The polders have also been criticized for their impact on coastal habitats and ecology (Roy et al., 2017).

Though these criticisms of polderization are widely reported (Alam et al., 2017; Auerbach et al., 2015; Tareq et al., 2018), it has proved difficult to provide quantified evidence of the effect of the coastal embankment programme because (i) the flooding processes are complex and derive from many sources and (ii) it is difficult to establish what the extent and severity of flooding might have been had the coastal embankments not been constructed. This paper seeks to address both of these challenges by (i) analysing past events to diagnose different types flooding and (ii) estimating the extent of flooding that could have occurred had the polders not been constructed. The first challenge is addressed through empirical analysis of the hydrometeorological factors that can explain the severity of observed floods, whilst the second is tackled by constructing models of different types of flooding.

2. Materials and methods

This research was conducted in two stages (Fig. 2). First, a series of flood observations for the years 1988-2012 were obtained from remote sensing imagery. Records of rainfall, river water level, and surge levels for the same period were used to identify the main type of flooding for each observed event. Second, the counter-factual scenario without the construction of coastal embankments was modelled in order to hypothesise how the flooding might have been different without the polders.

2.1. Flood hazard of south western coastal region of Bangladesh

The study addresses the south western coastal region of Bangladesh (Fig. 1) which is vulnerable to fluvio-tidal flooding, monsoonal precipitation induced pluvial flooding, and storm surges (Bhuiyan and Dutta, 2012; Gain et al., 2017). In the dry season, tidal oscillations dominate the low flows in the river channel in this region, making it susceptible to salt water intrusion. Before polder construction, a common practice from local people was to build temporary earthen embankments in the dry season to protect the land from salinity and remove those in wet season to enable sedimentation. Starting in 1960 a total of 44 polders were built in the Coastal Embankment Project (CEP) (Nowreen et al., 2014; Paul and Rashid, 2017), protecting 5187km^2 (WARPO, 2018). Polder construction transformed the coastal region into an agriculturally productive zone and encouraged people to settle within the polders (Nowreen et al., 2014). Conversely, polder construction de-linked the floodplain (Talchabhadel et al., 2016) and induced several problems including river flow reduction, siltation in tidal channels, drainage congestion, waterlogging, land subsidence, polder breaching, soil salinity, etc. (Auerbach et al., 2015; Choudhury et al., 2004; Gain et al., 2017; Nowreen et al., 2014; Paul and Rashid, 2017). For instance, polder construction has resulted in 1.0-1.5m of land subsidence inside an embanked area (Polder 32), whereas the outside of

this embankment, the neighbouring Sundarban mangrove forest, has remained comparatively unchanged (Auerbach et al., 2015).

In response to multifaceted problems related to polders, over the years the government of Bangladesh, in cooperation with various international donor agencies, have implemented several projects. The World Bank, who supported the CEP project, has started the Coastal Embankment Improvement Project (CEIP) Phase I in 2015, which is rehabilitating and/or reconstructing several polders, as well as upgrading the drainage channels and structures (Paul and Rashid, 2017). Meanwhile, the Blue Gold project, funded by Government of the Netherlands (GoN) and operated by the Bangladesh Water Development Board (BWDB), has been responsible for rehabilitation of water control structures within 26 polders districts (http://www.bluegoldbd.org/). In addition, Tidal River Management (TRM) has been adopted in an attempt to restore sedimentation within the polders through selective flooding (Van Staveren et al., 2017), gaining attention as a potential alternative to structural flood protection (Gain et al., 2017). The idea of TRM is to allow river flow into low-lying bowl-shaped depressions (termed as 'Beel') within polder for sediment deposition to fill those depressions (Masud et al., 2018; Van Staveren et al., 2017). Though historically a community driven approach, BWDB implemented TRM in several 'Beels' in 1991-2013 (Masud et al., 2018).

Despite several initiatives, the challenges of providing sustainable flood risk management in the south western polder region are intensifying, with the threat of sea level rise, upstream modification of river flows and sediments from the Ganges Brahmaputra Meghna river system, and high population density providing little space for adaptation (Haque et al., 2018; Kay et al., 2018).

2.2. Identifying flood events

In last two decades (Hoque et al., 2011), water surface detection through remote sensing techniques has become an essential tool for various disciplines (Sanyal and Lu, 2004; Sarp and Ozcelik, 2017). Among various methods, water-indexing techniques have proved to be very useful for quick flood detection (Sarp and Ozcelik, 2017). This study applied the Modified Normalized Difference Water Index (MNDWI) (Xu, 2006) using ArcGIS 10.6.1 to detect water surfaces during pre (dry) and post (wet) monsoon period in a year. MNDWI uses green and middle infrared (MIR) bands of Landsat satellite images. It generates positive values for water surfaces and negative values for built-up areas, soil surfaces and vegetation. Then a change detection algorithm was used in Geographic Information System (GIS) to identify cells that changed from being normally dry to wet, which were classified as flood cells for that year. Cloud cover during the monsoon period (May to September) (Ahmed and Akter, 2017) meant that the analysis was applied to compare pre and post monsoon images. The image database is summarised in Table S2 of the Supplementary Information.

The major cyclone Sidr in 2007 caused prolonged flooding within the polders (Tareq et al., 2018), which lasted into 2008. Hence using pre-monsoon images of 2008 could cause under estimation of flood extent in 2008, so dry season images from 2007 we employed to detect flood extent in both 2007 and 2008.

The accuracy of MNDWI based classified images was assessed, for three different years (1989, 2001, and 2010), against reference land cover data (classified and validated images) collected from Mukhopadhyay et al. (2018) (Table S1, supplementary document), producing an error matrix to estimate the overall accuracy and kappa statistics. The overall accuracy depicts a percentage agreement of pixels correctly classified (Lillesand et al., 2014). The kappa statistics (κ) is a measure for inter-rater reliability testing, whose value can range from -1 to +1, where ‘values ≤ 0 as indicating no agreement and 0.01–0.20 as none to slight,

147 0.21–0.40 as fair, 0.41– 0.60 as moderate, 0.61–0.80 as substantial, and 0.81–1.00 as almost
148 perfect agreement' (McHugh, 2012). The reference land cover data were converted into
149 binary images (water, dry) and classified dry season (pre-monsoon) images of those three
150 years were employed to estimate the indices of classification consistency. In this study,
151 'substantial agreement' within pixels between reference and classified land cover images
152 were found for 1989 and 2010, and 'almost perfect agreement' was achieved for 2001 image
153 classification (Table S3, supplementary document). The processed flood maps were used to
154 estimate the severity of observed flooding and also to validate the flood simulation outputs in
155 the second phase of the study. The reference land cover maps included 12 land use classes, in
156 which general waterbodies are separated from aquaculture, mixed agriculture/aquaculture and
157 agricultural lands. These maps were further used to analyse the types of land uses exposed to
158 pluvial flooding.

159 **2.3. Flood event classification**

160 To attribute the observed floods to different sources of flooding, we analysed the
161 severity of monsoon rainfall and elevated water levels within the region. Extreme value
162 analysis was conducted by fitting to a generalized extreme-value (GEV) distribution using the
163 L-moment method (Coles et al., 2001; Gilleland and Katz, 2016). The cumulative distribution
164 function of the GEV distribution is:

$$G(z) = \exp\left[-\left\{1 + \varepsilon\left(\frac{z-\mu}{\sigma}\right)\right\}_{+1}^{-1/\varepsilon}\right] \quad (1)$$

165 Where, z is the random variable (monsoon precipitation/peak river water level/peak
166 surge level) and ε, μ, and σ are the shape, location, and scale parameters respectively. The
167 return period (T) was estimated by following formula:

$$T = \frac{1}{1 - G(z)} \quad (2)$$

168 The precipitation frequency analysis was based on 10-days gridded precipitation data
169 from the Bangladesh Meteorological Department, aggregated into yearly monsoonal total

precipitation and computed the regional average from 1948-2012. Fluvio-tidal flood attribution was based on annual peak water level (Rao and Hamed, 2000), averaged across 18 river gauges. Finally, tidal surges were identified though analysis of peak tidal water level averaged across two tidal gauges in the Bay of Bengal, i.e. Hiron point and Khepupara (Fig. 1). Data used for flood frequency analysis are summarised in Table S1 of supplementary document.

In each year the return period of pluvial rainfall, fluvio-tidal water level and surge water level were estimated according to Equation 2, denoted T_p, T_f and T_s, respectively. We then sought to classify each year, estimating thresholds T_p', T_f' and T_s' above which a flood of the given type was said to have occurred and a flooded area A_f' which represented the threshold between 'flood' and 'non-flood' events. The thresholds were optimised according to the following criteria, applied in this order of priority:

1. The separation between 'flood' and 'non-flood' events should not be contradictory i.e. events cannot be classified as being a version of 'flood' (i.e. pluvial, fluvio-tidal or surge) and 'non-flood'.
2. If an event with multiple types flood is identified, the classification of flood event should be consistent with the ordering of severity of T, i.e. the classification should be of the event type with the greatest T.
3. All events with above average flooded area should be classified as a version of 'flood'.
4. The number of multiple classifications should be minimised.

If it is not possible to meet criteria 1-3 the number of constraint violations should be minimised.

193 **2.4. Modelling flood events**

194 **2.4.1. Pluvial flood model**

195 To simulate the effect of polders on pluvial flood severity, a simple pluvial flood
196 rainfall-runoff and spreading model was established. The model was then adjusted to
197 simulate the effects of subsidence and drainage system.

198 Pluvial flooding materialises based on the interaction between precipitation,
199 evapotranspiration, surface flow, local topography and drainage. It can occur either due to
200 intense downpours (Falconer et al., 2009; Houston et al., 2011) or by prolonged moderate to
201 heavy rainfall (Falconer et al., 2009). In low-lying areas like the polder region of south
202 western Bangladesh, these processes are extremely complex, so we have developed
203 simplified GIS-based water balance and flood spreading model to estimate inundated areas.

204 The Thornthwaite and Mather (TM) water balance model was used to produce
205 monthly excess precipitation grids. The water balance model takes gridded monthly total
206 precipitation (*P*), monthly mean temperature, monthly mean daylight hours, soil texture to
207 estimate monthly potential evapotranspiration (equation 3), monthly water deficit or excess
208 precipitation, actual evapotranspiration (equation 4, 5, 6, 7), and excess precipitation
209 (equation 8, 9, 10). Raster layers of potential evapotranspiration (PE) and monthly water
210 deficit or surplus (P-PE) in mm were calculated as follows:

$$PE_m = 16\ C \left(10\frac{T}{I}\right)^a \quad (3)$$

211 Where, T is the monthly average temperature (˚C), I is the annual heat index for the
212 year in concern, calculated as $I = \sum_1^{12} i$, where the monthly heat index $i = [T/5]^{1.514}$, $a =$
213 $6.75\times10^{-7}I^3 - 7.71\times10^{-5}I^2 + 1.792\times10^{-2}I + 0.49239$; the correction factor $C = m/30.d/12$,
214 where m is the number of days in the month and d is the monthly mean daylight hours (Singh
215 et al., 2004). The estimated monthly PE was then subtracted from the monthly P to find out
216 the water excess (+) or deficit (-). After that, the soil budget was estimated to find the actual

evapotranspiration. At this stage, a raster layer of available water capacity ($SOIL_{max}$) was created following Thornthwaite and Mather (1957) principles. As Dingman (2002) demonstrated,

If $P_m \geq PE_m$

$$SOIL_m = min\{[(P_m - PE_m) + SOIL_{m-1}], SOIL_{max}\} \quad (4)$$

$$AET_m = PE_m \quad (5)$$

If $P_m < PE_m$,

$$SOIL_m = SOIL_{m-1}\left[exp\left(\frac{P_m - PE_m}{SOIL_{max}}\right)\right] \quad (6)$$

$$AET_m = P_m + SOIL_{m-1} - SOIL_m \quad (7)$$

Where, AET_m is the actual evapotranspiration of the month in concern; $SOIL_{m-1}$ is the soil moisture content of previous month. To solve this recursive equation, the GIS toolset started running from the first month (when P-PE <0) after the monsoon, considering that the soil moisture storage in previous month (last month of monsoon) was full, i.e. equal to the estimated available water capacity. Next, the following conditions and equations were followed to estimate the monthly and monsoonal total excess precipitation (SUR).

If $(P\text{-}PE)_m<0$,

$$SUR_m = 0 \quad (8)$$

If $(P\text{-}PE)_m \geq 0$ and $SOIL_m = SOIL_{max}$,

$$SUR_m = (P - PE)_m \quad (9)$$

If $(P\text{-}PE)_m \geq 0$ and $SOIL_m \neq SOIL_{max}$,

$$SUR_m = (P - AET)_m + SOIL_m \quad (10)$$

Monsoon total excess precipitation,

$$SUR_Y = \sum SUR_{May\ to\ September} \quad (11)$$

The flood extent was estimated by considering a series of surface depressions, whose catchments are nested (Diaz-Nieto et al., 2011). The SRTM DEM was analysed to identify surface depressions, their exit points (points through which water will pass to next level depressions when a depression is full), and catchment areas. While identifying exit points, the model followed the single-direction flow algorithm (D8), where one cell routed into the next steepest of eight neighbouring cells (Seibert and McGlynn, 2007), and eliminated cells which drained back to the same depression. After that it selected depression points to define respective depressions catchments and nest levels were assigned for depression catchments.

The total volume of monsoon excess water from the water balance model was assigned to each depression. The water accumulation algorithm (equation 12) was started from the highest nest level depressions to accumulate water and subsequently passes to next level depressions. At this point, the model routes additional water, after filling previous level depressions (if remains), to the existing catchment(s). This iterative process continued until the model distributed water to the lowest nest level (Diaz-Nieto et al., 2011):

$$P_{P=0 \rightarrow P<0} = \sum P_{j=1,n} + E - V \quad (12)$$

Where, P = water volume passed down from depression, E = access volume after filling the depression, V = depression volume, j = counter of nested depressions from 1 to n.

For each year (1988-2012), the model was used to simulate pluvial inundation with and without polders. For pluvial inundation 'with' polders the observed DEM was used. Drainage from the polder was constrained due to inadequate maintenance of drainage channels and deterioration of sluice gates.

Brown and Nicholls (2015) documented 205 points measurements of net subsidence. Yearly land subsidence rates used in this study ranging from 0.24mm to 10mm per year. Using these point measurements, a raster of yearly subsidence rate was created, using Inverse Distance Weighted (IDW) interpolation. Multiplying this raster with subsequent number of years starting from 1960 (commencing year of polder construction) was added to the existing DEM to reconstruct past land elevations. The reconstructed DEM was used to delineate potential flood locations (surface depressions) in the 'without' polder scenario. The estimated total excess precipitation in each year was accumulated in the depressions and nested catchments. We further developed a scenario in which drainage channels within the polders were effectively maintained. These channels were identified by hand from the satellite image. Catchments that contained these channels were permitted to drain.

257 We performed sensitivity analyses for (a) the method used to interpolate land
258 subsidence rate (b) the rate of land subsidence, which was used to establish pluvial flood
259 model for the counterfactual scenario. First, using the observed land subsidence data we
260 generated three additional layers of land subsidence rates, applying kriging, spline, and
261 natural neighbour methods in GIS (Childs, 2004). These layers were incorporated to generate
262 pluvial flood inundation simulations for the 25 years studied for the counterfactual scenario.
263 We tested for significant differences in annual pluvial inundation in the counterfactual
264 scenario (Figure S1, supplementary document). This was done applying one-way analysis of
265 variance (ANOVA) test. An ANOVA test could be performed to measure the sensitivity of
266 input parameters (e.g. DEM) in hydraulic modelling and floodplain mapping (Raber et al.,
267 2007). The estimated *p*-value 0.22 indicated that the difference in inundation for four types of
268 land subsidence rates is not significant. The insignificant p-value and a smaller value of F-
269 ratio than the critical F-ratio (Table S4, supplementary document) confirmed the absence of
270 sensitivity in the pluvial flood model in relation to method applied to interpolate the rate of
271 land subsidence.

272 In addition, we generated raster layers of two land subsidence rates, randomly
273 splitting the observed 205 points measurements of net subsidence rate into two groups. The
274 first group contained a subset of 70% points, whereas the second group was comprised of the
275 remaining 30% points. Yearly land subsidence rates in the two groups ranging from 1mm to
276 10mm and 1mm to 6mm, respectively. We applied IDW interpolation method to obtain two
277 layers of subsidence rates, which were added (multiplying by the difference of modelled year
278 from 1960) separately on the existing DEM to generate two different surfaces. We
279 incorporated these surfaces in pluvial flood model to estimate the inundated area across
280 delineated depressions. Here, we modelled the pluvial events of 2004 and 2006, when a
281 higher amount of excess precipitation was estimated (Fig. 6). Figure S2 in supplementary

document exhibits a similar pattern of individual depression behaviour for a change in land subsidence rate. Again, ANOVA test was performed to analyse the difference in inundation during two events in individual depression, for different rates of land subsidence. The obtained p-value 0.27 and F-ratio 1.3 (< critical F-ratio 2.01) indicated that the difference in inundation in different depressions insignificant.

The pluvial flood model was validated based on a field survey that was conducted on May 2018 to collect GPS locations of pluvial floods and non-floods (Figure S3, supplementary document). An error matrix was produced (Table S5, supplementary document) to verify the accuracy of modelled potential flood/non-flood pixels, comparing to observations. An overall accuracy of 95% and spatial statistical κ statistics value 0.87 suggest an 'almost perfect agreement' (McHugh, 2012) between observed and modelled flood pixels.

The observed total inundation in years that were identified as pluvial flood events were plotted against the modelled inundation of corresponding years for 'with polder' scenario, yielding a coefficient of determination R^2=0.98 (Fig. 3). However, the validation process also included 2005 event, despite it was classified as 'no flood' event. The reason for using this event to validate the pluvial flood model is explained in Section 3.3.

2.4.2. Fluvio-tidal and storm surge inundation model

The Delft 3D hydrodynamic model (Haque et al., 2018) was used to estimate inundation extent from fluvio-tidal (1998) and storm surge flooding (2007) for 'with' and 'without' polder scenarios. The model domain was bounded by border with India in the west (type of boundary is not fixed), Lower Meghna estuary in the east, three major rivers (Ganges, Brahmaputra and Upper Meghna) in the north and Bay of Bengal in the south. The discretized model domain contains 896,603 grid points, where grid size varies from 186m to 1704m. Coarser grid size is provided in the ocean and finer grid size is provided in the river channels to capture the details of the river/estuarine systems and topographic variation. The

307 model was set up for all rivers and estuaries with a width of at least 100m. Measured flow
308 data was provided from BWDB for three the major rivers, from which fluvial flow enters the
309 model. In absence of measured sea level data, the model takes simulated sea level data from
310 the GCOMS model (Kay et al., 2015), which generated the tidal (ocean) boundary. As
311 morphological changes were considered static (except subsidence) – no additional sediment
312 input is provided. A rate of 2.6 mm/yr (Brown and Nicholls, 2015) of subsidence is
313 considered in the area bounded by the polders including the polder itself. A DEM with a
314 spatial resolution of 50m was provided by WARPO (2018). The ocean bathymetry data was
315 obtained from General Bathymetric Chart of the Oceans (GEBCO) while river bathymetry
316 data was collected from BWDB at 294 locations in coastal rivers/estuaries. Channel
317 planforms were assumed to remain the same over the model simulation period. Similar
318 assumption was made for channel bed level and floodplain levels of rivers / estuaries.
319 The model indirectly considered impacts of land use and land cover through
320 resistance in the floodplain. Different resistance values were specified for sea,
321 rivers/estuaries, floodplain and forest (Sundarban). These resistance values were determined
322 during model calibration. The calibrated Manning's roughness coefficient was spatially
323 variable having values of 0.00025 in the ocean (considered as large water body), 0.015 to
324 0.025 in rivers /estuaries (a value generally considered to be valid for rivers / estuaries in the
325 region), 0.025 to 0.040 in the floodplain, and 0.08 to 0.1 in forests including mangrove and
326 natural plantation. The model simulated 103 polder areas (out of 139) using design heights of
327 embankments collected from BWDB. Present day observations are only available for 61
328 polders (some of which are outside the study region) that show that actual polder heights can
329 vary from 3m to 7m (Huq et al., 2010). Where actual embankment heights are not available,
330 an average design embankment height of 4.75m is used in the model (CEIP, 2013). Storm
331 surge modelling was based on a reconstructed cyclone track for the 2007 cyclone Sidr (Figure

S4, supplementary document) that passed by the study area. Consideration of reconstructed cyclone track was based on the premise that modelled result could ideally explain the observed flood inundation. Resulting simulated inundation data was masked for the south western polder region. Further details on model setup, calibration, and validation can be found in Haque et al. (2018) and Haque and Rahman (2016).

3. Results and discussion

3.1. Identification of flood events

In 25 observed years, the inundated area ranged from 6% (in 2010) to 48% (in 2001). The mean flood footprint was 13% of the total embanked region. The patterns of inundation were heterogeneous spatially and temporally, with different parts of the embanked region flooded in different years. Six polders were flooded by more than 13% (average flood area) of their respective area, on average. The largest extent of inundation occurred in polder 34/1, whereas the polder 28/2 and 30 experienced the lowest level of inundation (Figure S5, supplementary document).

Fig. 7(a) shows a typical inundation footprint for the year 2004 obtained from remote sensing data analysis. Here, major inundation occurred in the northern segment of embanked region. Generally, flooding in the south western part of the region was less frequent and the extent of inundation in that segment was relatively low during various events.

3.2. Classification of flood events

3.2.1. Frequency analysis

Fig. 4 portrays the frequency analysis of total monsoon precipitation, peak river water level, and peak surge level respectively to classify them into pluvial, fluvio-tidal, and surge induced floods. The estimated return periods of these three hydrological parameters varied annually, indicating different types of floods in different years. For instance, within 25 observed years, the highest monsoon precipitation was in 2002, whereas the highest peak

river water level and surge level were in 1996 and 2007 respectively. The relationship between flood conditioning factors and flood type is complex (Nied et al., 2014), in this study, we provide a simplified flood classification system estimating minimum thresholds T_p', T_f' and T_s'.

3.2.2. Flood event classification

Table 1 presents the return period of each type of flood in each year. The optimisation of return periods of three hydrological parameters yielded the following minimum flood thresholds: T_p'= 5.2 years, T_f'= 5.9 years and T_s'= 7.9 years and threshold between 'flood' and 'non-flood' events was 10.3% of the area. According to this criterion, floods were identified as occurring in 14 different years and three compound events were detected. The estimated thresholds generated one false negative and one false positive flood event. The event in 1996 was classified as 'F' even though the flood area was 9.2%. The highest T_f during that event was responsible for such attribution. Besides, 2005 event was classified as 'N' despite about 11.5% area was inundated. In 2005, the region received a lower level of monsoon precipitation, in addition to low peak river water level and surge level. The outcome of pluvial flood model explained the reason for a higher level of inundation in 2005 (Section 4.3).

We find that pluvial flooding was the most frequent, but typically resulted in less flooded area (11.4% of the region on average) compared with the other forms of flooding. The fluvio-tidal and surge induced floods caused more extensive inundation than the pluvial floods: 21.8% and 30.2% on average, respectively. The greatest area of inundation (48% of total area) occurring in 2001 as a consequence of fluvio-tidal and surge flooding, whilst cyclone Sidr in 2007 flooded 35% of the area.

Fig. 5(a) illustrates the identified pluvial floods. We classified seven pluvial flood events considering 5.2-year return period as the minimum threshold level. The region

382 received the highest monsoonal precipitation of 1861.91mm in 2002 leading to an 18.8-year
383 return level of pluvial flood. The highest two precipitation events in 2002 and 2011 caused
384 approximately 11% of total polder area inundation, while 2004 resulted in the highest pluvial
385 inundation (13% area).

386 The six events that were classified as fluvio-tidal happened in 1995, 1996, 1998,
387 2000, 2001, and 2002. The highest regional average peak water level of 3.45m was observed
388 in 1996, leading to a 34.6-year event (Fig. 5(b)). But the most extreme event did not result in
389 the highest extent of inundation. For instance, whilst in 1996 the inundation area was 9%, the
390 highest percentage of total area (48%) was inundated in 2001 when the region experienced a
391 23-year fluvio-tidal flood which breached various polders. However, the 2001 event was
392 attributed to both the fluvio-tidal and surge event, though fluvio-tidal flood was the dominant
393 force (as higher return period) leading to the inundation. Fluvio-tidal floods mostly occurred
394 in between 1995 and 2002. After 2003, relatively a lower mean discharge in upper Ganges
395 River was observed (Figure S6, supplementary document), contributing to a lower peak river
396 water level.

397 Four surge induced floods were attributed, considering the estimated 7.9-year return
398 period as minimum threshold limit (Fig. 5(c)). The most extreme surge occurred in 2007
399 during the cyclone Sidr, when the peak surge height reached to 4.16m (35-year return
400 period), causing 35% of the total area inundation. Another major cyclone Aila affected the
401 study area in 2009 with a peak surge of 4.10m, leading to 21% area inundation. Both fluvio-
402 tidal and surge flooding formed the compound event of 1995, when the impact of surge was
403 the highest.

404 **3.3. Modelling flood inundation with and without polders**

405 The outcome of pluvial flood model indicated that the study area was prone to pluvial
406 inundation annually, since excess precipitation of different magnitude was estimated in all

407 studied years (Fig. 6). The extent of inundation has a strong positive correlation with the
408 amount of excess precipitation (correlation coefficient = 0.90). Among the classified seven
409 pluvial flood events (Table 1), the lowest level of monsoon precipitation was observed in
410 2004. But, the greatest extent of pluvial inundation was estimated in 2004, due to presence of
411 the highest amount of excess precipitation caused by a lower level of evapotranspiration. In
412 2005, the modelled pluvial inundation was 11.2% area, which is similar to observed flood
413 inundation (11.5%) for that year. The lowest level of evapotranspiration was estimated in
414 2005, leading to a higher amount of excess precipitation. Therefore, the extent of inundation
415 in 2005 was greater than A_f' (10.3%), despite the region received a 1.2-year return level
416 precipitation. Thus, we included this event to validate the outcome of pluvial flood modelling
417 (Section 2.4.1). The results from pluvial flood modelling further demonstrated that a greater
418 extent of inundation was the outcome of polder construction and inadequate drainage
419 systems. The extent of pluvial inundation would have been substantially lower in absence of
420 polders.

421 Typical results from the pluvial flood model are shown in Fig. 7(b, c), which
422 illustrates how a combination of land subsidence (a maximum of approximately 0.5m relative
423 to locations where polders were not constructed) and inadequate drainage, has exacerbated
424 pluvial flooding. We estimate that on average over the modelled period the extent of flooded
425 area was 334km^2 (i.e. 6.5% of total area) larger because of the land subsidence, generated
426 from the construction of polders, and inadequate drainage. The extent of inundation primarily
427 depends on the number of surface depressions generated due to land subsidence. Polder
428 construction increased the number of shallow depressions (<1m in depth), which are prone to
429 flooding. Without polders flooding in those areas might have been alleviated, as
430 sedimentation would have transformed the geomorphology of the region and reduced the
431 number of shallow depressions. Flooding in that case would have only occurred in areas

characterized as deep surface depressions. Hence, our modelled pluvial inundation for the counter-factual scenario showed relatively a small year-to-year difference in the extent of inundation (Fig. 6), although the total inundated area was positively correlated with the estimated excess precipitation.

Results from the pluvial flood model further indicated that if the observed drainage system were maintained adequately, it would have been able to reduce pluvial flooding by about 4.9%. This number is relatively small because there are many catchments that were not observed to have a drainage channel. The pluvial flood prone area comprises about 50% aquaculture land (shrimp culture and freshwater fish culture), which is not necessarily harmfully affected by flooding. However, 40% of the flood-prone area is agricultural land (rice field, other croplands, mixed rice and shrimp culture) which can be more adversely impacted by pluvial flooding, whilst 10% is comprised of settlement areas with homestead vegetation where pluvial flooding is directly harmful.

Simulations of fluvio-tidal and surge flooding demonstrate the effectiveness of embankments in reducing inundation due to elevated water levels. For example, during the 1998 fluvio-tidal flood, majority of the region would have been flooded without polders. The presence of polders resulted in an estimated 27% of total area being flooded in this fluvio-tidal flood, compared to 79% for the 'without polder' counter-factual. Complete inundation occurred in 14 polders for 'with' polder scenario, which would have been escalated to 31 polders for the counter-factual scenario (Fig. 8(a)). Overlaying the inundated areas for both scenarios, we found that the embankments protected an estimated 54% area from flooding.

Simulation results for surge event Sidr suggests that, in presence of polders (without breaching), about 18% of the total area might have been inundated. Without polders, the extent of inundation would have been increased to approximately 35% area. Seventeen different polders that were partially at risk of flooding would have been inundated by more

than 80% area without embankments (Fig. 8(b)). However, our modelled total inundation for counter-factual scenario is similar to the observed inundation of 35% area. When simulating inundation for 'with polder' scenario, the model considered overtopping as the flood mechanism in polders. Therefore, the number of flood-affected polders were substantially lower under this scenario. But, embankment failure in several polders, both in form of damage and overtopping, increased the extent of inundation. Furthermore, the observed inundation in 2007 is a compound inundation of pluvial and surge induced flooding. The estimated pluvial inundation in 2007 was about 10% area. Subtracting (spatially) the pluvial inundation from the observed inundation, we found that surge induced flood solely contributed to the inundation in 25% area.

4. Conclusion

Creation of polders by construction of embankments in coastal Bangladesh has been a controversial process. The creation of polders enabled large increases in agricultural production and reduced the impacts of storm surges and fluvio-tidal floods. However, blocking off the coastal floodplain from channels practically eliminated annual deposition of sediments on the land, whilst compaction of sediment and anthropogenic activities exacerbated land subsidence. Over the years, drainage channels have not been adequately maintained, which has inhibited drainage of pluvial flood waters and exacerbated inundations. Moreover, construction of polders has provided an impression of security from flood hazards, encouraging human settlement in vulnerable locations.

In this paper we have empirically analysed the evidence for both the beneficial and harmful impacts of polder construction. We found that pluvial flooding occurs frequently, but the flood extent is usually less than in other forms of flooding. By modelling a counter-factual scenario in which polders had not been constructed we quantified a substantial (6.5%

481 area) increase in pluvial flooding that can be attributed to land subsidence resulted from
482 polder construction and poor management of drainage facilities.

483 On the other hand, the polders have provided protection against fluvio-tidal and storm
484 surge events. In the worst fluvio-tidal flood in the 'without polder' scenario 79% of the area
485 would have been flooded, compared with 27% which occurred with the polders. In the surge
486 event Sidr, 18% of the polder area would have been flooded, without the breaching to
487 embankments. But, the extent of inundation was increased to 25% area due to the damage to
488 embankments during the cyclone. Simultaneously, pluvial flooding exacerbated the flood
489 impact, inundating a total 35% area in 2007.

490 The empirical analysis of past floods reported in this paper is subject to errors in
491 observations of precipitation and water levels. In addition, the recognition of flooded areas
492 from satellite imagery is also subject to error. The attribution of flood types is to some extent
493 subjective, based on the criteria that were used to optimise the classification thresholds.
494 Given the relatively short record of flood events, the complexity of the flooding process and
495 the possibility of compound events, it would not be possible to establish a definitive
496 classification method.

497 Flooding processes in low-lying coastal areas are complex, so the modelling we have
498 used to analyse the 'without polder' counter-factual is inevitably approximate. This
499 particularly applies to pluvial flooding, which is sensitivity to local rainfall patterns,
500 topography, land surface and drainage and so would be extremely difficult to model with
501 more accuracy on the spatial/temporal scale considered in this study. Nonetheless, these
502 models have provided insights into the polders' effectiveness. Generally, this study is an
503 attempt to estimate the impact of anthropogenic intervention (creation of coastal
504 embankments) on the hydrology (inundation) of south western embanked region of
505 Bangladesh.

Rehabilitation and reconstruction of embankments is now under way in the coastal zone of Bangladesh (Figure S8, supplementary document). Further choices will need to be made in the face of rising sea levels. Alternative adaptation strategies are being examined as part of the Bangladesh Delta Plan. The empirical analysis of the benefits and impacts of embankment construction, which has been reported in this paper, should help to inform plans for adaptation of Bangladesh's coastal zone to flood hazards, by helping to target and sequence investments for flood management.

Acknowledgement

This work is an output from the REACH programme (www.reachwater.org.uk) funded by UK Aid from the UK Department for International Development (DFID) for the benefit of developing countries (Aries Code 201880). However, the views expressed, and information contained in it are not necessarily those of or endorsed by DFID, which can accept no responsibility for such views or information or for any reliance placed on them. We thank the anonymous reviewers for their careful reading of our manuscript and insightful comments and suggestions.

5. References

Abdullah AYM, Masrur A, Adnan MSG, Baky MAA, Hassan QK, Dewan A. Spatio-Temporal Patterns of Land Use/Land Cover Change in the Heterogeneous Coastal Region of Bangladesh between 1990 and 2017. Remote Sensing 2019; 11: 790.

Abedin MA, Shaw R. The role of university networks in disaster risk reduction: Perspective from coastal Bangladesh. International Journal of Disaster Risk Reduction 2015; 13: 381-389.

Ahmed KR, Akter S. Analysis of landcover change in southwest Bengal delta due to floods by NDVI, NDWI and K-means cluster with landsat multi-spectral surface reflectance

satellite data. Remote Sensing Applications: Society and Environment 2017; 8: 168-181.

Akber MA, Khan MWR, Islam MA, Rahman MM, Rahman MR. Impact of land use change on ecosystem services of southwest coastal Bangladesh. Journal of Land Use Science 2018; 13: 238-250.

Alam MS, Sasaki N, Datta A. Waterlogging, crop damage and adaptation interventions in the coastal region of Bangladesh: A perception analysis of local people. Environmental Development 2017; 23: 22-32.

Auerbach LW, Goodbred SL, Jr., Mondal DR, Wilson CA, Ahmed KR, Roy K, et al. Flood risk of natural and embanked landscapes on the Ganges-Brahmaputra tidal delta plain. Nature Climate Change 2015; 5: 153-157.

Bamberg S, Masson T, Brewitt K, Nemetschek N. Threat, coping and flood prevention – A meta-analysis. Journal of Environmental Psychology 2017; 54: 116-126.

Bhuiyan MJAN, Dutta D. Analysis of flood vulnerability and assessment of the impacts in coastal zones of Bangladesh due to potential sea-level rise. Natural Hazards 2012; 61: 729-743.

Brammer H. Bangladesh's dynamic coastal regions and sea-level rise. Climate Risk Management 2014; 1: 51-62.

Brouwer R, Akter S, Brander L, Haque E. Socioeconomic Vulnerability and Adaptation to Environmental Risk: A Case Study of Climate Change and Flooding in Bangladesh. Risk Analysis 2007; 27: 313-326.

Brown S, Nicholls RJ. Subsidence and human influences in mega deltas: The case of the Ganges–Brahmaputra–Meghna. Science of The Total Environment 2015; 527-528: 362-374.

554 CEIP. Technical feasibility studies and detailed design for Coastal Embankment
555 Improvement Programme (CEIP). Ministry of Water Resources, Government of the
556 People's Republic of Bangladesh, Dhaka, 2013.
557 Childs C. Interpolating surfaces in ArcGIS spatial analyst. ArcUser, July-September 2004;
558 3235: 569.
559 Choudhury NY, Paul A, Paul BK. Impact of costal embankment on the flash flood in
560 Bangladesh: A case study. Applied Geography 2004; 24: 241-258.
561 Coles S, Bawa J, Trenner L, Dorazio P. An introduction to statistical modeling of extreme
562 values. Vol 208: Springer, 2001.
563 Diaz-Nieto J, Lerner DN, Saul AJ, Blanksby J. GIS Water-Balance Approach to Support
564 Surface Water Flood-Risk Management. Journal of Hydrologic Engineering 2011; 17:
565 55-67.
566 Dingman SL. Physical hydrology: Waveland Press, 2002.
567 Falconer R, Cobby D, Smyth P, Astle G, Dent J, Golding B. Pluvial flooding: new
568 approaches in flood warning, mapping and risk management. Journal of Flood Risk
569 Management 2009; 2: 198-208.
570 Gain AK, Benson D, Rahman R, Datta DK, Rouillard JJ. Tidal river management in the south
571 west Ganges-Brahmaputra delta in Bangladesh: Moving towards a transdisciplinary
572 approach? Environmental Science and Policy 2017; 75: 111-120.
573 Gilleland E, Katz RW. Extremes 2.0: an extreme value analysis package in r. Journal of
574 Statistical Software 2016; 72: 1-39.
575 Haque A, Kay S, Nicholls RJ. Present and Future Fluvial, Tidal and Storm Surge Flooding in
576 Coastal Bangladesh. Ecosystem Services for Well-Being in Deltas. Springer, 2018,
577 pp. 293-314.

578 Haque A, Nicholls RJ. Floods and the Ganges-Brahmaputra-Meghna Delta. Ecosystem
579 Services for Well-Being in Deltas. Springer, 2018, pp. 147-159.
580 Haque A, Rahman M. Flow Distribution and Sediment Transport Mechanism in the Estuarine
581 Systems of Ganges-Brahmaputra-Meghna Delta. International Journal of
582 Environmental Science and Development 2016; 7: 22.
583 Hoque R, Nakayama D, Matsuyama H, Matsumoto J. Flood monitoring, mapping and
584 assessing capabilities using RADARSAT remote sensing, GIS and ground data for
585 Bangladesh. Natural Hazards 2011; 57: 525-548.
586 Houston D, Werritty A, Bassett D, Geddes A, Hoolachan A, McMillan M. Pluvial (rain-
587 related) flooding in urban areas: the invisible hazard. York: Joseph Rowntree
588 Foundation 2011.
589 Hui R, Jachens E, Lund J. Risk-based planning analysis for a single levee. Water Resources
590 Research 2016; 52: 2513-2528.
591 Huq M, Khan MF, Pandey K, Ahmed MMZ, Khan ZH, Dasgupta S, et al. Vulnerability of
592 Bangladesh to cyclones in a changing climate: potential damages and adaptation cost:
593 The World Bank, 2010.
594 Islam M, Kotani K, Managi S. Climate perception and flood mitigation cooperation: A
595 Bangladesh case study. Economic Analysis and Policy 2016a; 49: 117–133.
596 Islam MA, Mitra D, Dewan A, Akhter SH. Coastal multi-hazard vulnerability assessment
597 along the Ganges deltaic coast of BangladesheA geospatial approach. Ocean &
598 Coastal Management 2016b; 127: 1-15.
599 Kay S, Caesar J, Janes T. Marine Dynamics and Productivity in the Bay of Bengal.
600 Ecosystem Services for Well-Being in Deltas. Springer, 2018, pp. 263-275.
601 Kay S, Caesar J, Wolf J, Bricheno L, Nicholls RJ, Saiful Islam AKM, et al. Modelling the
602 increased frequency of extreme sea levels in the Ganges-Brahmaputra-Meghna delta

due to sea level rise and other effects of climate change. Environmental Sciences: Processes and Impacts 2015; 17: 1311-1322.

Khan MMH, Bryceson I, Kolivras KN, Faruque F, Rahman MM, Haque U. Natural disasters and land-use/land-cover change in the southwest coastal areas of Bangladesh. Regional Environmental Change 2015; 15: 241-250.

Lillesand T, Kiefer RW, Chipman J. Remote sensing and image interpretation: John Wiley & Sons, 2014.

Masud MMA, Moni NN, Azadi H, Van Passel S. Sustainability impacts of tidal river management: Towards a conceptual framework. Ecological Indicators 2018; 85: 451-467.

McHugh ML. Interrater reliability: the kappa statistic. Biochemia Medica 2012; 22: 276-282.

Moniruzzaman M. Impact of Climate Change in Bangladesh: Water Logging at South-West Coast. In: Leal Filho W, editor. Climate Change and the Sustainable Use of Water Resources. Springer Berlin Heidelberg, Berlin, Heidelberg, 2012, pp. 317-336.

Mukhopadhyay A, Hornby DD, Hutton CW, Lázár AN, Amoako Johnson F, Ghosh T. Land Cover and Land Use Analysis in Coastal Bangladesh. In: Nicholls RJ, Hutton CW, Adger WN, Hanson SE, Rahman MM, Salehin M, editors. Ecosystem Services for Well-Being in Deltas: Integrated Assessment for Policy Analysis. Springer International Publishing, Cham, 2018, pp. 367-381.

Nied M, Pardowitz T, Nissen K, Ulbrich U, Hundecha Y, Merz B. On the relationship between hydro-meteorological patterns and flood types. Journal of Hydrology 2014; 519: 3249-3262.

Nishat A, Nishat B, Abdullah Khan MF. A Strategic View of Land Management Planning in Bangladesh. Flood Risk Science and Management, 2010, pp. 484-498.

627 Nowreen S, Jalal MR, Khan MSA. Historical analysis of rationalizing South West coastal
628 polders of Bangladesh. Water Policy 2014; 16: 264-279.
629 Paul BK, Rashid H. Climatic Hazards In Coastal Bangladesh - Non-Structural and Structural
630 Solutions. Cambridge, United States: Elsevier, 2017.
631 Raber GT, Jensen JR, Hodgson ME, Tullis JA, Davis BA, Berglund J. Impact of LiDAR
632 nominal post-spacing on DEM accuracy and flood zone delineation. Photogrammetric
633 engineering & remote sensing 2007; 73: 793-804.
634 Rahman R, Salehin M. Flood Risks and Reduction Approaches in Bangladesh. In: Shaw R,
635 Mallick F, Islam A, editors. Disaster Risk Reduction Approaches in Bangladesh.
636 Springer, Tokyo, 2013, pp. 65-90.
637 Rao AR, Hamed K. Flood frequency analysis. USA: CRC press, 2000.
638 Roy K, Gain AK, Mallick B, Vogt J. Social, hydro-ecological and climatic change in the
639 southwest coastal region of Bangladesh. Regional Environmental Change 2017; 17:
640 1895-1906.
641 Sanyal J, Lu XX. Application of remote sensing in flood management with special reference
642 to monsoon Asia: A review. Natural Hazards 2004; 33: 283-301.
643 Sarp G, Ozcelik M. Water body extraction and change detection using time series: A case
644 study of Lake Burdur, Turkey. Journal of Taibah University for Science 2017; 11:
645 381-391.
646 Seibert J, McGlynn BL. A new triangular multiple flow direction algorithm for computing
647 upslope areas from gridded digital elevation models. Water Resources Research 2007;
648 43.
649 Singh RK, Hari Prasad V, Bhatt CM. Remote sensing and GIS approach for assessment of the
650 water balance of a watershed. Hydrological Sciences Journal 2004; 49: 131-142.

651 Talchabhadel R, Nakagawa H, Kawaike K. Tidal River Management (TRM) and Tidal Basin
652 Management (TBM): A case study on Bangladesh. E3S Web of Conferences. 7, 2016.
653 Tareq SM, Tauhid Ur Rahman M, Zahedul Islam AZM, Baddruzzaman ABM, Ashraf Ali M.
654 Evaluation of climate-induced waterlogging hazards in the south-west coast of
655 Bangladesh using Geoinformatics. Environmental Monitoring and Assessment 2018;
656 190: 230.
657 Thornthwaite CW, Mather JR. Instructions and tables for computing potential
658 evapotranspiration and the water balance. Drexel Institute of Technology, Centerton,
659 NJ (EUA). Laboratory of Climatology, 1957.
660 Van Staveren MF, Warner JF, Khan MSA. Bringing in the tides. from closing down to
661 opening up delta polders via Tidal River Management in the southwest delta of
662 Bangladesh. Water Policy 2017; 19: 147-164.
663 WARPO. National Water Resources Database(NWRD). Water Resources Planning
664 Organization (WARPO), Bangladesh, 2018.
665 Xu H. Modification of normalised difference water index (NDWI) to enhance open water
666 features in remotely sensed imagery. International Journal of Remote Sensing 2006;
667 27: 3025-3033.

Table 1. Flood attribution in south western polder region

Year	Precipitation return period (T_p)	Return period of peak river water level (T_f)	Surge peak return period (T_s)	Percentage of area inundated (A_f)	Flood type (P-Pluvial, F-Fluvio-tidal, S-Surge, N-No flood)
1988	9.5	3.9	6.5	10.3	P
1989	1.4	1.5	2.7	6.5	N
1990	2.1	2.1	2.4	9.3	N
1991	1.7	1.6	1.9	8.2	N
1992	1.3	3.4	2.5	7.8	N
1993	8.1	1.8	1.5	11.4	P
1994	1.3	1.2	1.2	5.9	N
1995	2.8	6.4	13.4	16.5	F, S
1996	1.4	34.6	4.3	9.2	F
1997	2.2	1.9	2.1	9.3	N
1998	3.0	11.8	2.0	22.8	F
1999	7.9	3.6	1.8	10.8	P
2000	2.9	8.2	5.0	10.9	F
2001	1.7	22.7	9.2	48.1	F, S
2002	18.8	12.3	1.5	10.7	P, F
2003	1.1	5.8	2.2	7.9	N
2004	5.2	1.3	1.0	13.1	P
2005	1.2	1.2	1.1	11.5	N
2006	5.7	1.6	1.2	13.0	P
2007	3.0	2.4	34.9	35.0	S
2008	1.4	1.5	2.8	10.1	N
2009	1.6	4.4	22.8	21.2	S
2010	1.1	1.0	1.2	6.1	N
2011	11.8	1.1	1.2	10.8	P
2012	1.1	1.1	1.1	7.0	N

Fig. 1. South western embanked region of Bangladesh

Fig. 2. Analytical process of this study

Fig. 3. Modelled versus observed pluvial flood inundation plot

Fig. 4. Return level plots with fitted GEV df and 95% confidence bands

Fig. 5. Classified flood events in relation to values corresponding hydrological parameters

Fig. 6. Simulated pluvial flood inundation for three scenarios

Fig. 7. Impact of polders on pluvial flooding (2004 event)

Fig. 8. Polder wise inundation in two scenarios during (a) fluvio-tidal flood of 1998, and (b) storm surge flood of 2007

Fig.1

Click here to download high resolution image

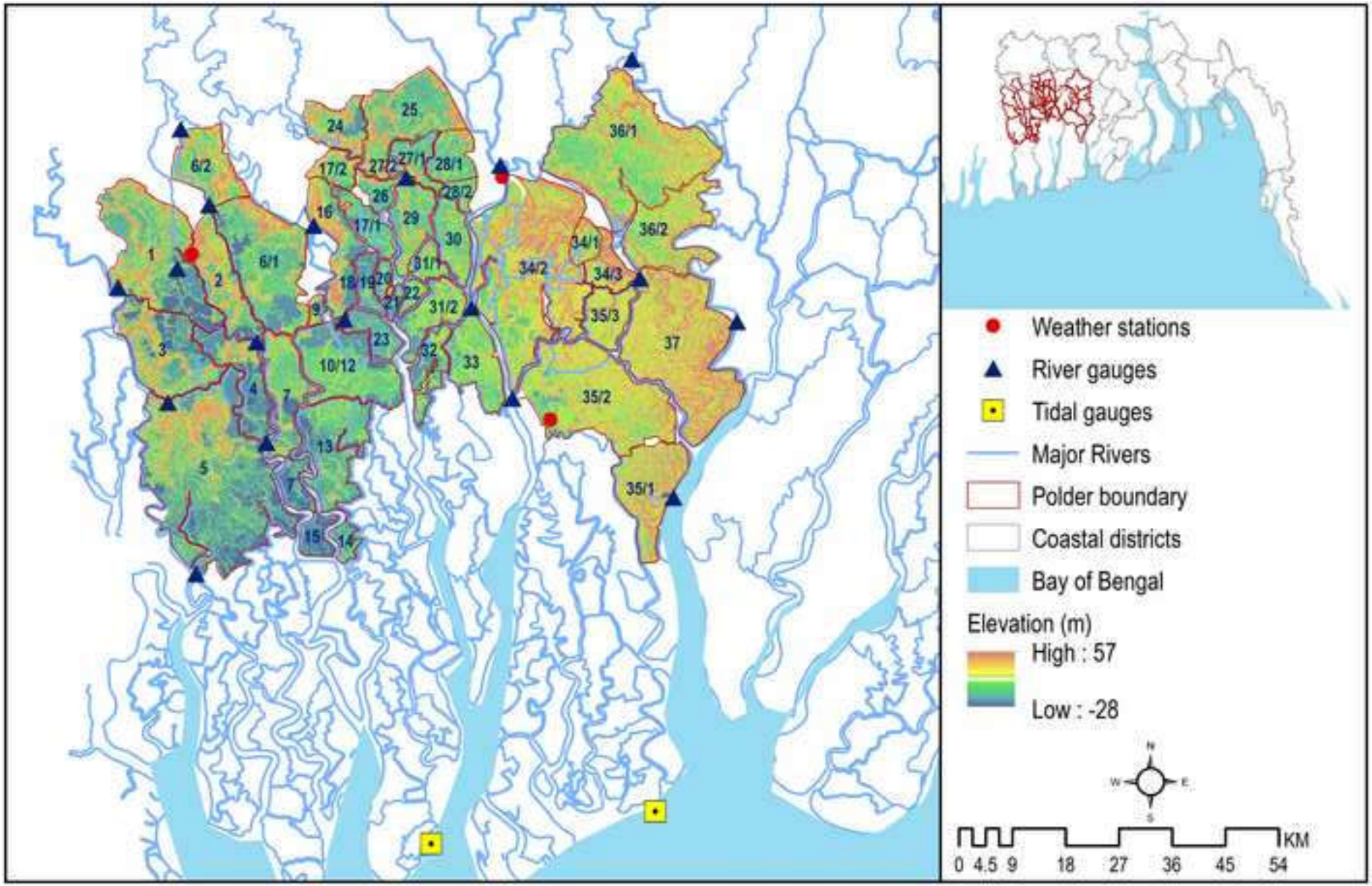

Fig.2

Click here to download high resolution image

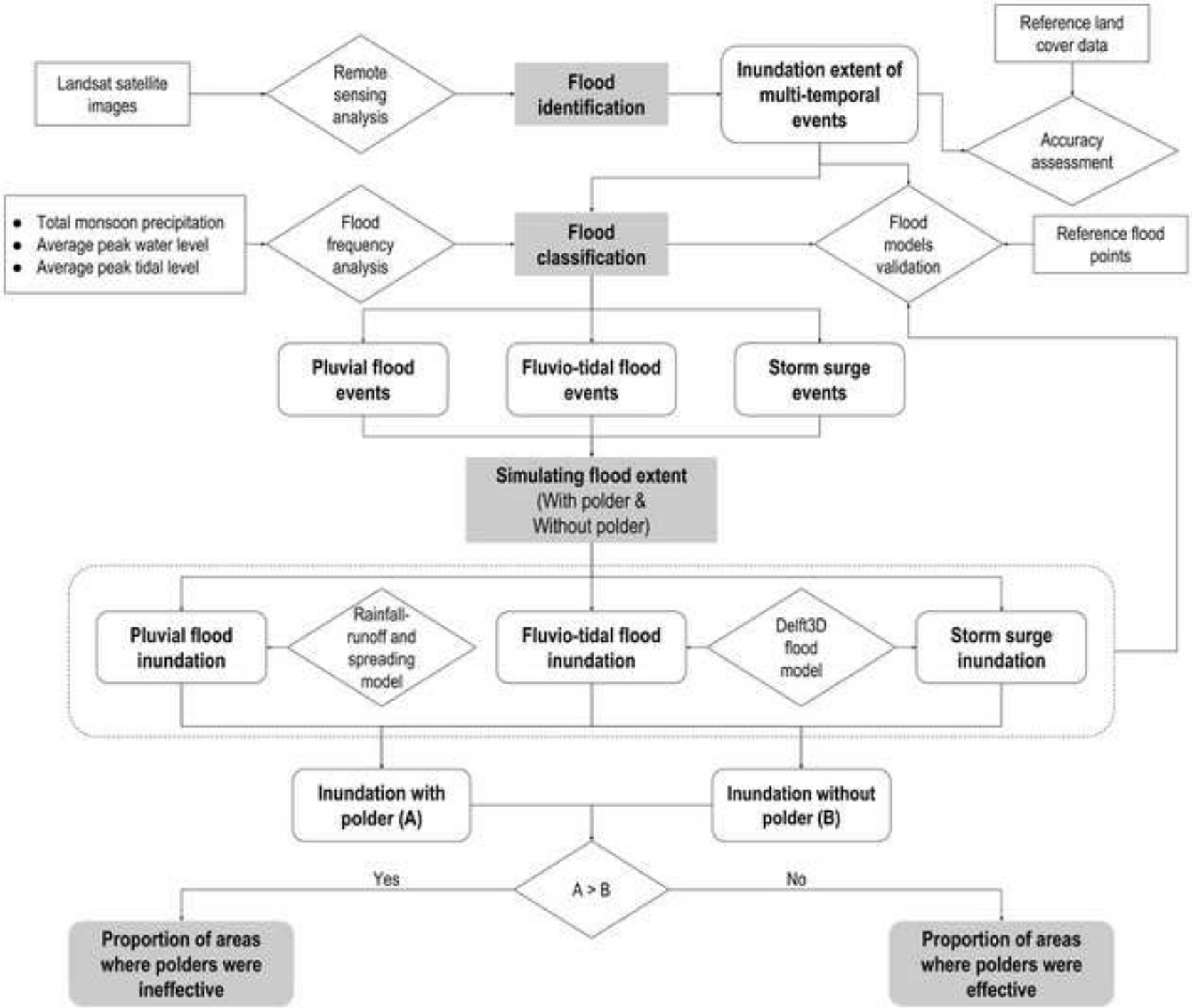

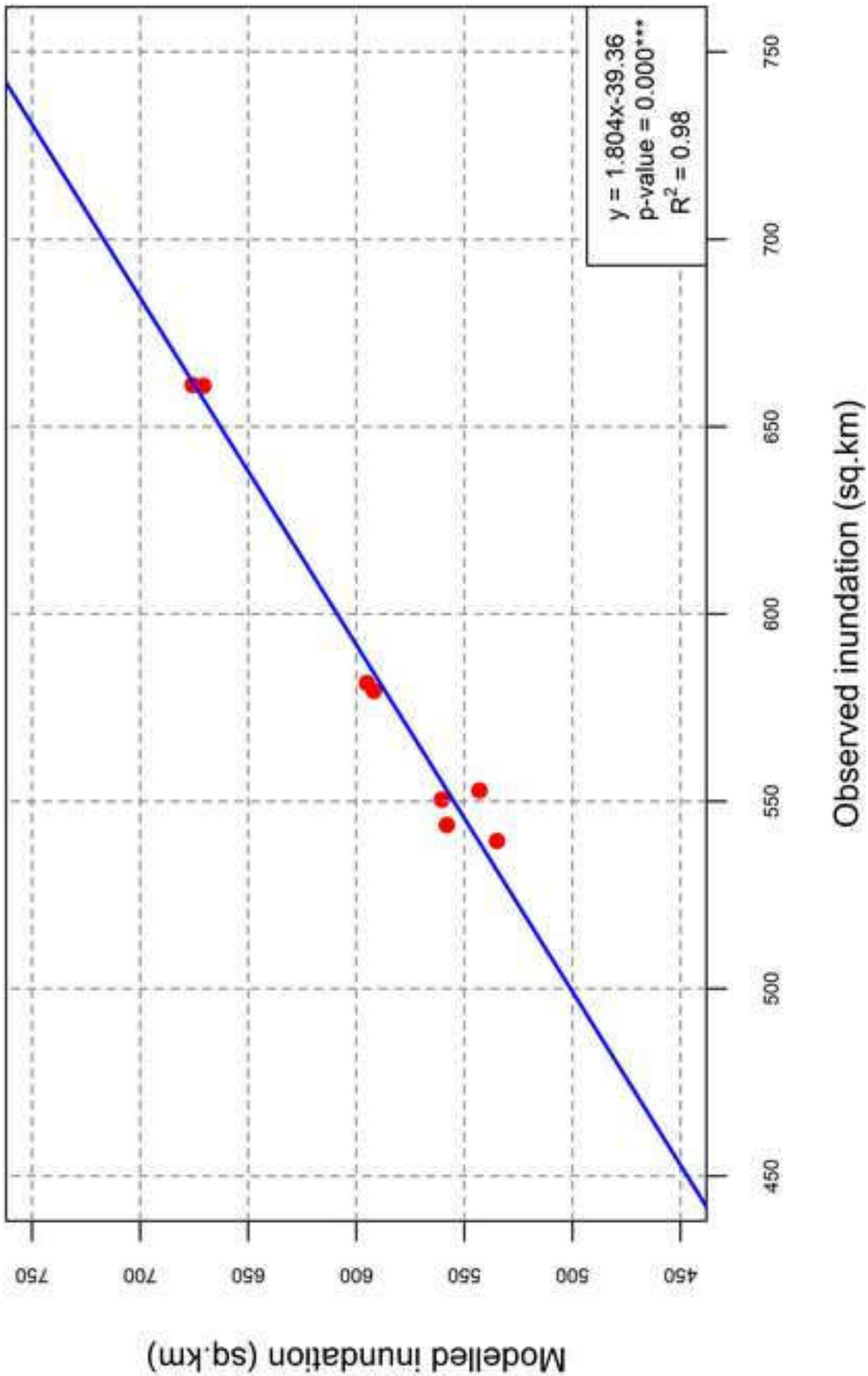

Fig.3
Click here to download high resolution image

Fig.4

Click here to download high resolution image

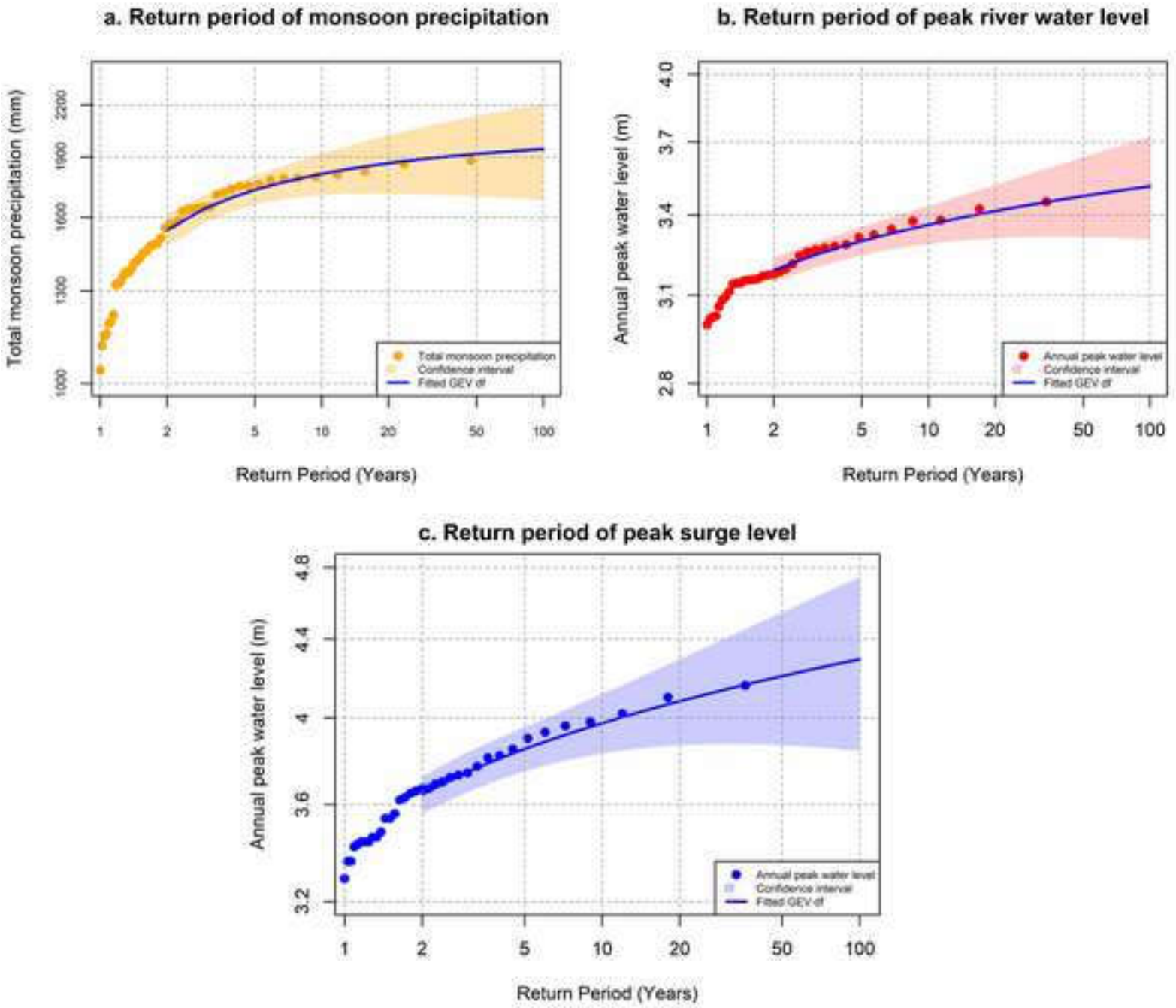

Fig.5

Click here to download high resolution image

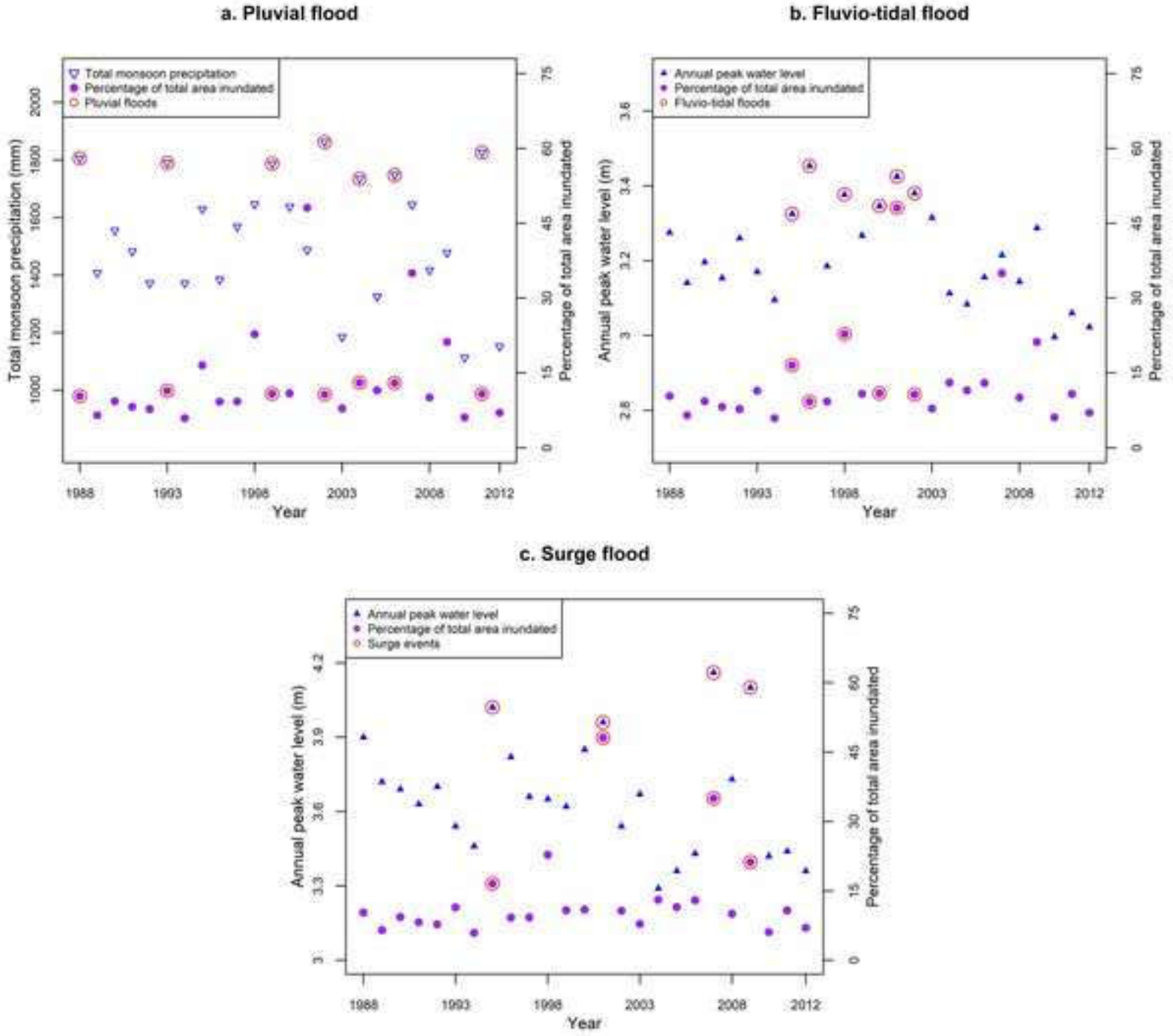

Fig.6

Click here to download high resolution image

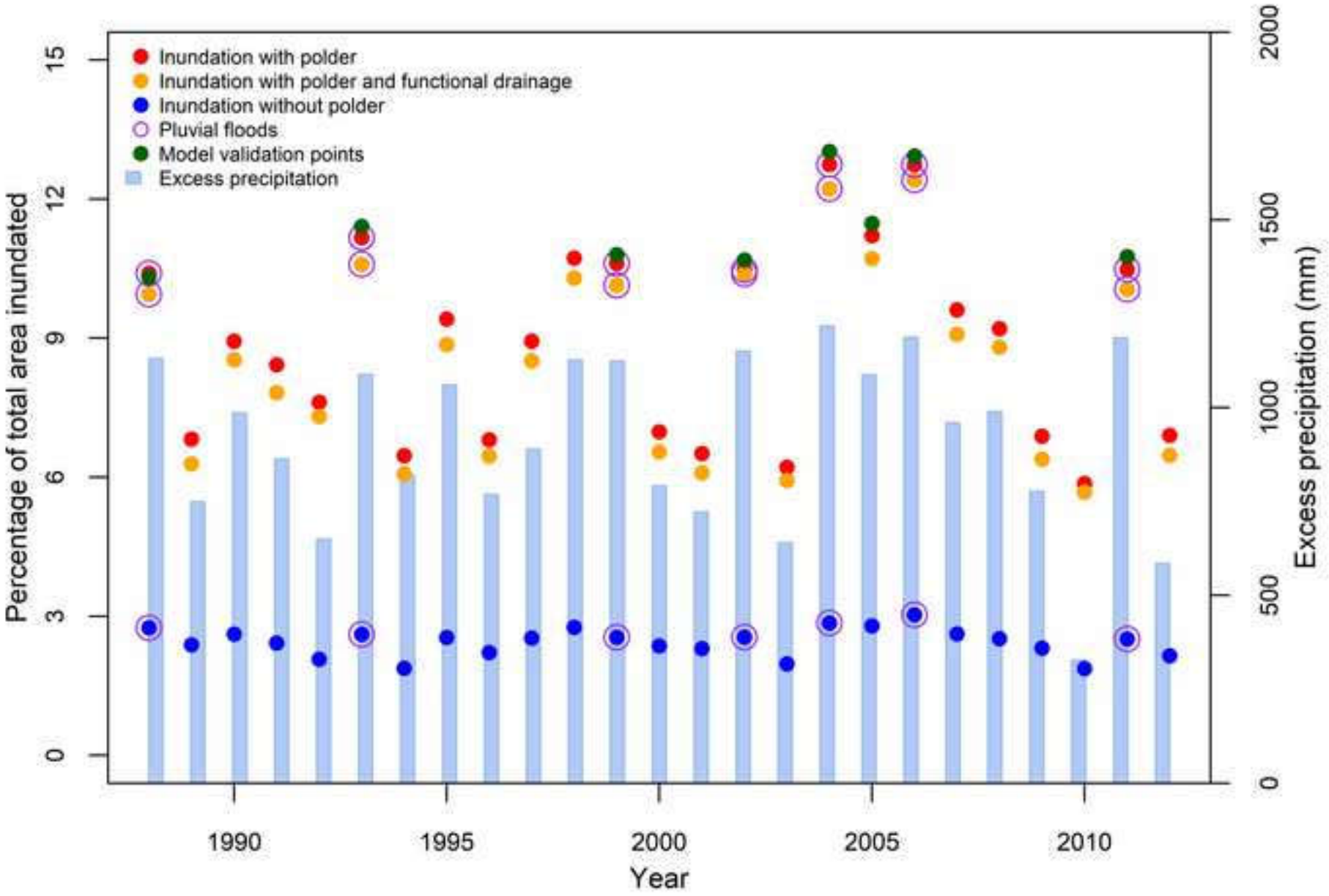

Fig.7

Click here to download high resolution image

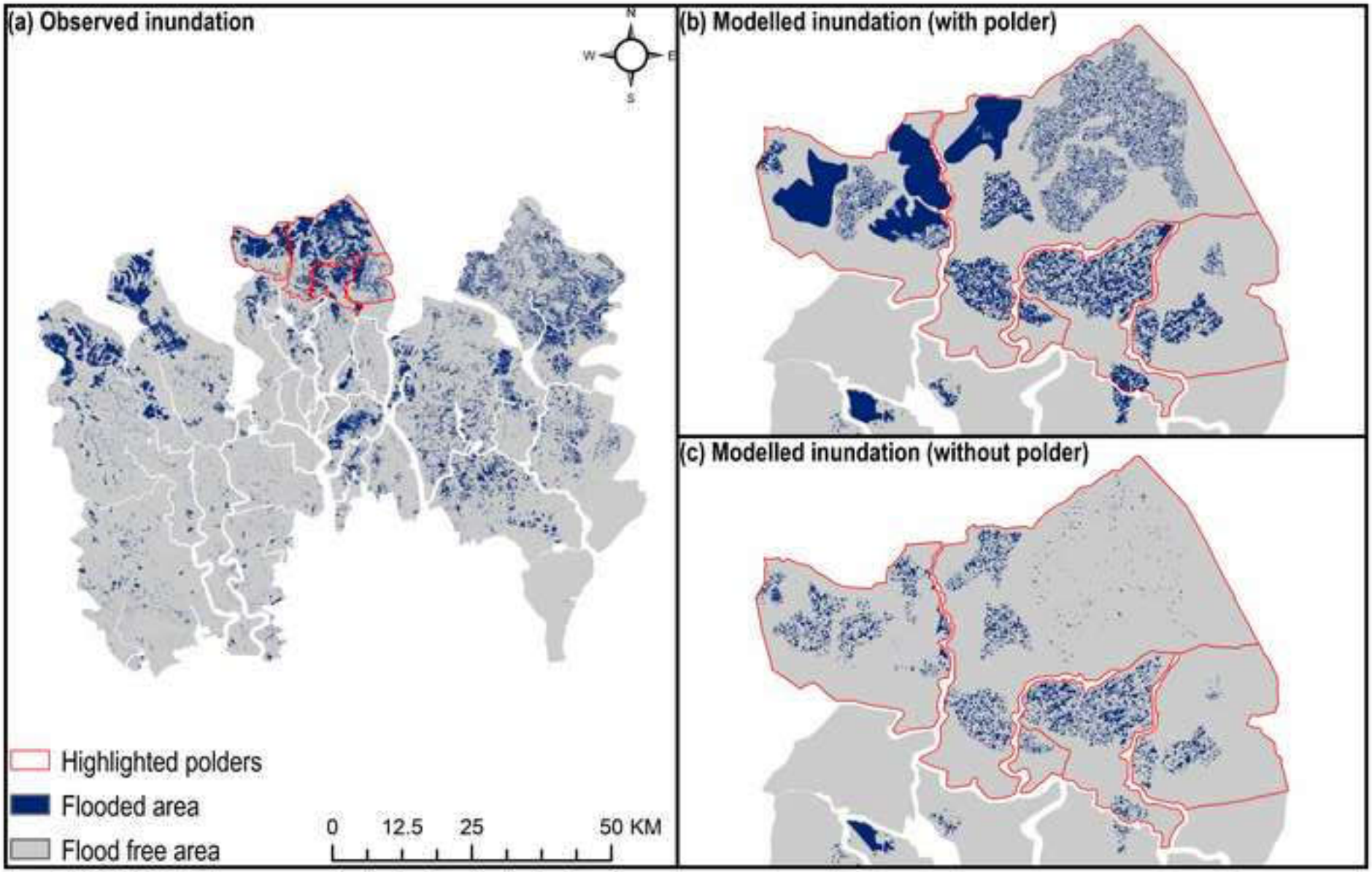

Fig.8

Click here to download high resolution image

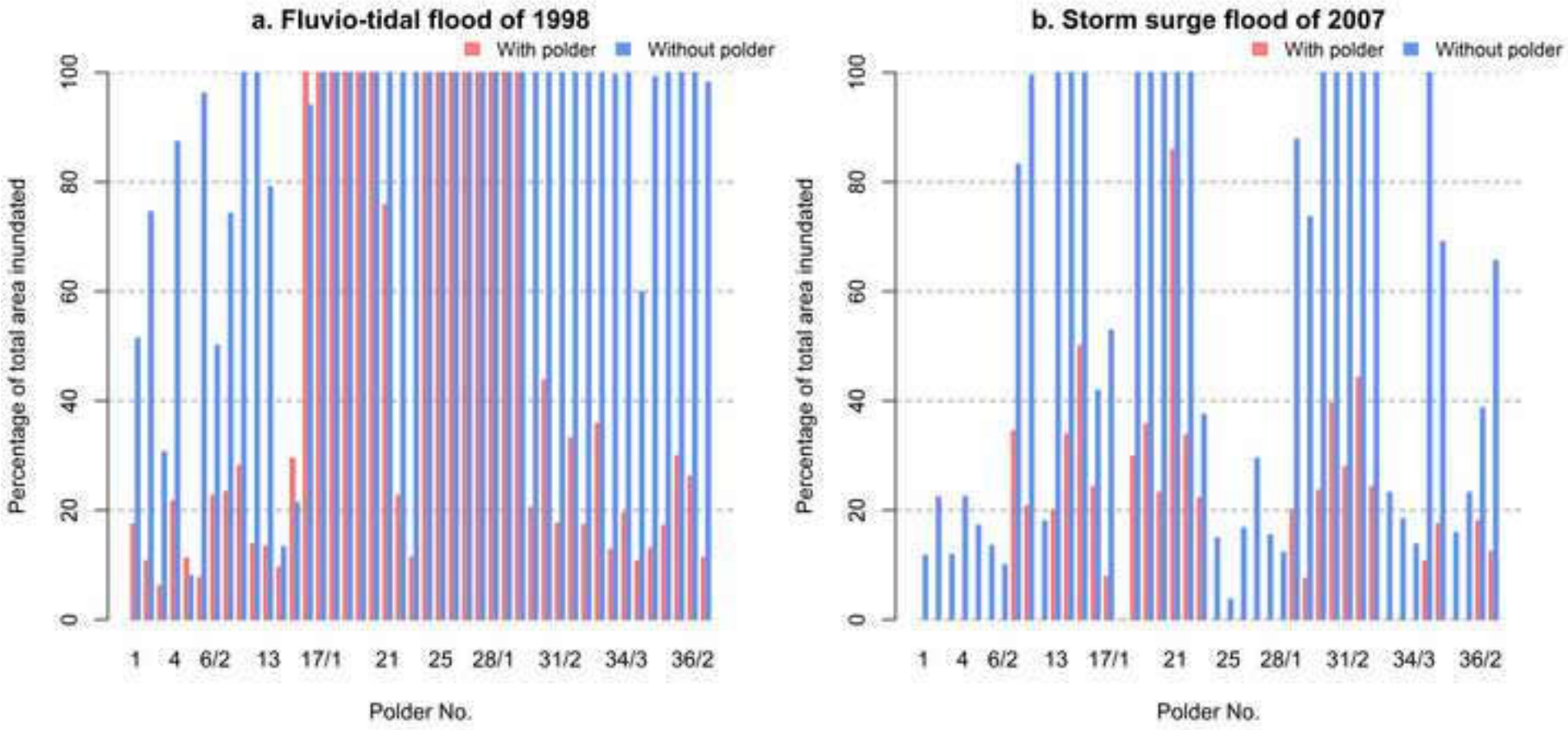

Supplementary material for on-line publication only

Click here to download Supplementary material for on-line publication only: Supplementary document.docx